Reaction channel contributions to the triton optical potential

N. Keeley*
National Centre for Nuclear Research, ul. Andrzeja Sołtana 7, 05-400 Otwock, Poland

R. S. Mackintosh†
School of Physical Sciences, The Open University, Milton Keynes MK7 6AA, England, United Kingdom

(Received 8 October 2020; accepted 26 October 2020; published xxxxxxxxxx)

Background: Well-established coupled-channel (CC) and coupled reaction channel (CRC) processes make contributions to elastic scattering that are absent from local density folding models. Little is known concerning the contribution of these processes to ^{3}H optical model potentials. For studying such processes, spin-saturated closed-shell nuclei such as ^{16}O and ^{40}Ca are particularly suitable target nuclei and the (^{3}H, ^{4}He) reaction is easily handled within conventional reaction theory since it avoids complications such as breakup.
Purpose: To establish and characterize the contribution to the ^{3}H-nucleus interaction generated by coupling to proton pickup (outgoing ^{4}He) channels; we also study the contribution of collective states and identify effects of dynamical nonlocality due to these couplings.
Methods: CRC calculations, with CC coupling to collective states, provide the elastic channel S matrix S_{lj} resulting from the included processes. Inversion of S_{lj} produces a local potential that yields, in a single channel calculation, the elastic-scattering observables from the CC/CRC calculation. Subtracting the bare potential yields a local and l-independent representation of the dynamical polarization potential (DPP). From the DPPs due to a range of channel couplings the influence of dynamically generated nonlocality can be identified.
Results: Coupling to ^{4}He channels systematically induces repulsion and absorption in the ^{3}H optical model potential (OMP) and generally a reduction in the rms radius of the real part. The qualitative effects, including the general undularity of the DPPs, are similar for all cases. Such coupling cannot be represented by renormalizing folding model potentials. Evidence is presented for substantial dynamical nonlocality of the induced DPPs. Local equivalent DPPs for individual couplings cannot be added to give the DPP for multiple couplings.
Conclusions: The DPPs presented here further challenge the notion that local density folding models provide a satisfactory description of elastic scattering from nuclei. Coupling to proton pickup channels induces dynamical nonlocality in the ^{3}H OMP with implications for direct reactions involving ^{3}H. Departures from a smooth radial form for the ^{3}H OMP should be found in good fits to suitable elastic-scattering data.

DOI: 10.1103/PhysRevC.00.004600

I. INTRODUCTION

Collective and reaction channel processes play an essential role in direct nuclear reactions [1]. In particular, these processes make an important contribution to the simplest direct reaction: elastic scattering. This contribution is not represented in theories of the nuclear optical model based on local density models. The formal contribution of such processes to the nucleon optical model potential (OMP) is both nonlocal and l dependent [1–3]. The nonlocality referred to here is distinct from the nonlocality due to exchange processes and will be referred to as dynamical nonlocality in what follows. However, such processes can be represented as a local and l-independent contribution to the phenomenological OMP in a way briefly reviewed in Sec. II A.

In this paper we study the contribution of coupling to transfer channels and collective excitations to the ^{3}H OMP. The calculations presented here for ^{3}H projectiles are as close as possible to similar calculations performed previously for ^{3}He projectiles [4]. Apart from the various points of interest in the comparison of the interactions of the pair ^{3}H and ^{3}He on a doubly closed-shell nucleus, we are concerned to put beyond doubt the essential contributions of the coupling effects that we study. These contributions have no representation in current folding models based on local density approximations. Their phenomenological representation requires either angular momentum dependence or undularity. The results presented here imply that some representation of transfer and inelastic processes should not be excluded from future models of nuclear scattering.

The contribution of coupled reaction channels to the OMP has been studied for protons (for recent contributions see [5–9]), deuterons [10], and helions [4] but in all these cases many effects were omitted or treated incompletely. For example, in the case of the contribution of neutron pickup (PU) to proton scattering, the breakup of the deuteron was generally not taken into account. In this respect, the contribution of the coupling of ^{4}He channels to the ^{3}H OMP is favorable, and is studied in this paper, along with the contribution of collective

*nicholas.keeley@ncbj.gov.pl
†raymond.mackintosh@open.ac.uk

excitation of the target nucleus. A substantial contribution of nucleon pickup coupling to the mass-3 OMP was found long ago [11], but that work has been superseded by major improvements to coupled reaction channel (CRC) codes: finite range coupling and nonorthogonality corrections are included in the FRESCO code [12] employed in the present paper.

In Ref. [4], a considerable contribution from coupling to inelastic and pickup channels was found for the ^{3}He OMP for target nuclei ^{16}O and ^{40}Ca. The present paper applies the same methodology to the ^{3}H OMP for the same nuclei for the following reasons.

(1) There is a substantial contribution that is very different from a renormalization of a folding model potential. This commonly ignored situation is worthy of being firmly established.

(2) The difference between the ^{3}He and ^{3}H OMP for $T = 0$ target nuclei is of interest: for example, the difference between ^{3}He and ^{3}H OMPs can be used to determine the $\boldsymbol{t} \cdot \boldsymbol{T}$ term for $T \neq 0$ target nuclei.

(3) The influence of coupling effects is likely to be easier to identify empirically for doubly closed-shell nuclei for which the potentials differ most markedly from global optical model potentials. Moreover, more good data exist for such nuclei.

(4) The contributions of the inelastic and transfer processes for ^{3}He projectiles strongly suggested L dependence and dynamical nonlocality, two properties which, once established, must propagate into any future models of elastic scattering.

The departure from global trends of the OMPs for closed-shell nuclei was established for ^{3}He projectiles by Pang *et al.* [13]. Moreover, elastic-scattering angular distributions for closed-shell target nuclei tend to have deeper minima, making them harder to fit with standard parametrized forms. These facts make scattering from such nuclei of particular interest in the quest to understand interactions between nuclei. Moreover ^{16}O and ^{40}Ca are both spin-saturated nuclei. Information concerning the spin-orbit interaction for ^{3}H scattering from nuclei is sparse, while that for helion scattering is the subject of a theoretical and phenomenological review by Hanspal *et al.* [14]. These authors distinguish the contribution of the spin saturated core and the contribution of the other target nucleons. This makes the interpretation of scattering from spin-saturated nuclei, such as ^{16}O and ^{40}Ca, more straightforward. Comparison of ^{3}H and ^{3}He interactions for such $T = 0$ targets potentially facilitates the identification of consequences for isospin symmetry breaking.

II. INELASTIC AND PICKUP CONTRIBUTIONS TO THE ^{3}H OMP

A. Determining coupling contributions to the OMP

The channel coupling contributions to the ^{3}H OMP are determined as follows: the elastic channel S matrix S_{lj} from a coupled channel (CC) calculation (CC refers throughout to both collective and reaction channel couplings) is subject to $S_{lj} \rightarrow V(r) + \mathbf{l} \cdot \mathbf{s} V_{\rm SO}(r)$ inversion [15], and the difference between the resulting potential and the "bare potential," the elastic channel potential of the CC calculation, is identified as a local representation of the dynamical polarization potential (DPP), due to the coupling; see Ref. [16] for more details.

In contrast to the local DPPs determined by inversion, the formal DPP is both l dependent and nonlocal (see Refs. [1–3,17]). This channel-coupling nonlocality is distinct from the nonlocality due to exchange [18], the consequences of which are commonly represented phenomenologically [19,20]. We refer to the nonlocality arising from channel coupling as *dynamical nonlocality*, and evidence for it will be presented in what follows, exploiting the nonadditivity of the local-equivalent DPPs as discussed in Refs. [16,17,21]. Some of the undulatory ("wavy") properties of the local and l-independent DPPs found by inversion can be attributed to the underlying l dependence of the formal DPP [1–3]. In what follows all CC calculations were performed with the code FRESCO [12].

The dynamical nonlocality generated by channel coupling has an important consequence: the local equivalent DPP due to the coupling to a number of states when included in a single CC calculation is not the sum of the local equivalent DPPs that would be found when each of the coupled states was included in a separate CC calculation (see Refs. [16,17] and also Ref. [21] for further discussion). The consequences of this motivate a number of the comparisons described in this paper. One immediate consequence is that the local DPP due to a number of coupled states cannot be calculated as the sum of the local DPPs due to each of the states coupled individually.

B. The coupling, inelastic and (^{3}H, ^{4}He) transfer

1. *Scattering from* ^{16}O

The contributions of coupling to the following states were studied: (1) the $\frac{1}{2}^-$ ground state of ^{15}N (the Q value for pickup to this state is 7.6865 MeV); (2) the $\frac{3}{2}^-$ state of ^{15}N at 6.3238 MeV; and (3) the collective 3^- state of ^{16}O at 6.130 MeV. The collective coupling effect was evaluated in a separate calculation and also together with the pickup coupling. Of primary interest, of course, is the contribution to the DPP of all the couplings together. However, as well as the interest in the distinctive contributions of collective and transfer coupling, there is significance in the degree to which contributions to the DPP add (or, rather, do not add) together. As discussed in earlier works [16,17], the nonadditivity of such contributions to the local equivalent DPPs gives a measure of the dynamical nonlocality generated by the coupling.

For the PU calculations, the $\langle ^4\text{He} \mid ^3\text{H} + p \rangle$ overlap, i.e., the $p + ^3$H binding potential and spectroscopic factor, were taken from Brida *et al.* [22]. For the targetlike overlaps, the $p + ^{15}$N binding potentials and spectroscopic factors were taken from Flavigny *et al.* [23], which fitted the magnitude of the forward angle (^{3}H, ^{4}He) pickup data of Pinder *et al.* [24] for the transition populating the 0.0-MeV $\frac{1}{2}^-$ state of ^{15}O. The exit channel ^{4}He $+^{15}$N optical potentials were calculated using the global parameter set of Ref. [25]. For the inelastic excitations, the $B(E3; 0^+ \rightarrow 3^-)$ was taken from Ref. [26] and the corresponding nuclear deformation length δ_3 was taken from Ref. [27]. The full complex remnant term and nonorthogonality correction were included in the PU calculations.

2. *Scattering from* ^{40}Ca

We studied the contributions to elastic scattering of coupling to the following pickup and collective states.

Pickup coupling was included to all states of ^{39}K with spectroscopic factors greater than 0.1, as determined in the paper by Doll *et al.* [28], some 18 states in all. Data are available for (^{3}H, ^{4}He) pickup to the 0.0-MeV $3/2^+$ level of ^{39}K for an incident ^{3}H energy of 33 MeV [24]. The Q value for pickup to the ground state of ^{39}K is 11.4857 MeV.

Collective coupling was included to two states of ^{40}Ca: the 3^- state at 3.737 MeV and the 2^+ state at 3.9044 MeV.

Like the case of scattering from ^{16}O, the dynamical nonlocality generated by the coupling is probed by examining the additivity of various contributions, pickup and inelastic, to the local equivalent DPP.

The pickup calculations again used the $\langle ^4\mathrm{He} \mid ^3\mathrm{H} + p\rangle$ overlap of Brida *et al.* [22] while the $p + ^{39}$K binding potentials were taken from Doll *et al.* [28]. The corresponding spectroscopic factors were also taken from Doll *et al.* except for the transition to the 0.0-MeV $3/2^+$ level of ^{39}K where the Doll *et al.* value was multiplied by a factor of 0.9 to provide the best description of the data of Pinder *et al.* [24] for (^{3}H, ^{4}He) pickup to this state. The exit channel ^{4}He $+^{39}$K optical potentials were calculated using the global parameter set of Ref. [25]. For the inelastic excitations, $B(E3; 0^+ \rightarrow 3^-)$ and $B(E2; 0^+ \rightarrow 2^+)$ were taken from Refs. [26,29], respectively, and the corresponding nuclear deformation lengths, δ_3 and δ_2, were taken from Ref. [30].

III. FITS TO ELASTIC-SCATTERING DATA

In order to study the contributions of various combinations of collective and/or reaction channel couplings, we first determine the ^{3}H potentials that fit the elastic-scattering differential cross sections from ^{16}O and ^{40}Ca when all couplings to the pickup and collective states of the target nuclei, as listed in the previous section, are included. We refer to the resulting potentials as the bare potentials for ^{16}O and ^{40}Ca. No analyzing power data are available for ^{3}H incident on ^{16}O or ^{40}Ca targets at the required energy, 33 MeV. The geometries of the spin-orbit terms of the optical potentials were therefore held fixed at the ^{3}He values found in our previous work [4] and only the depths were searched. The DPPs arising from particular couplings are found by subtracting the bare potential, for each radial point, from the potential that exactly reproduces the elastic channel S_{lj}, and thus the elastic channel observables, for a coupled-channel calculation for those particular couplings with the bare potential. It was shown in Ref. [8] that the DPPs are not strongly dependent on the bare potential. All the DPPs for different couplings for the ^{16}O and ^{40}Ca cases are calculated with fixed bare potentials, determined as above, for the respective ^{16}O and ^{40}Ca target nuclei.

Figure 1 compares the fit to the elastic scattering of ^{3}H from ^{16}O [31] with the couplings all switched on, solid lines, and with the bare potential (all couplings switched off), dashed lines. It is clear that the couplings substantially influence the angular distribution as far forward as 30°. The effect is very similar to what was found for the corresponding case for ^{3}He [4].

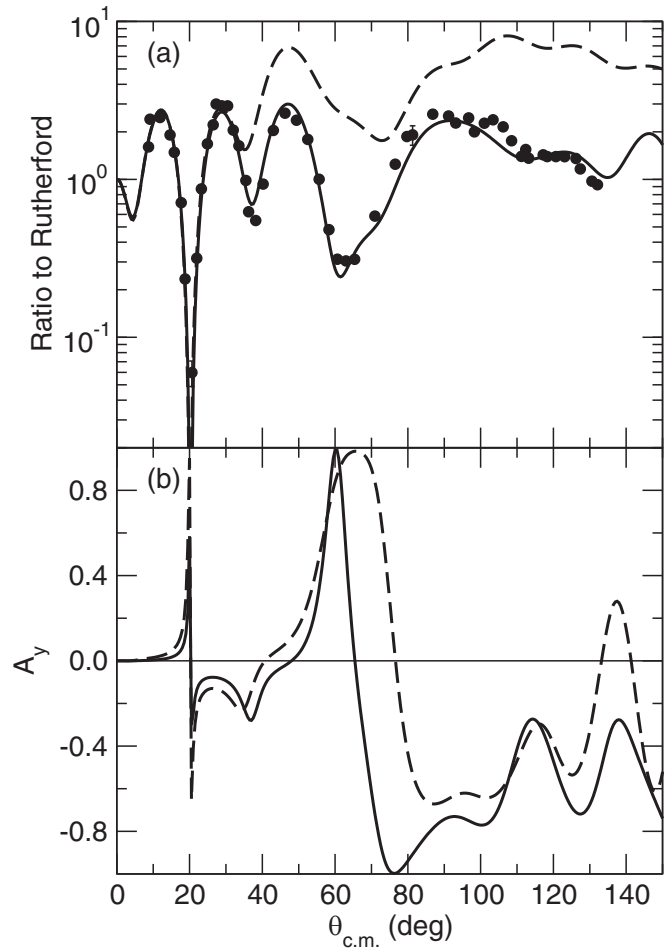

FIG. 1. For 33-MeV ^{3}H on ^{16}O, the solid lines are the differential cross-section (a) and analyzing power (b) angular distributions for the full coupled-channel calculation with fitted optical model parameters. The dashed lines are calculated with the same potential (the bare potential) but with no coupling. The data are from Ref. [31].

Figure 2 compares the fit to the elastic scattering of ^{3}H from ^{40}Ca [31] with the couplings all switched on, solid lines, and with the bare potential (all couplings switched off), dashed lines. The difference would be experimentally significant from about 40° but becomes about an order of magnitude beyond 60°, again similar to the effect for ^{3}He [4].

Finally, we present in Fig. 3 the potential obtained by inversion of the full CC calculation S matrix S_{lj} for the case of 33-MeV ^{3}H on ^{16}O. The dashed lines in this figure present the four components of the bare potential corresponding to the dashed lines in Fig. 1. The local potential that fits the data, obtained by inversion and corresponding to the full set of channel couplings (pickup and inelastic), is given by the solid lines in Fig. 3. A full discussion of the channel couplings will be presented in what follows, but here we note three clear effects.

(1) The real central potential has imposed undularity (waviness) though the rms radius and volume integral have properties in line with systematics, as discussed below.

(2) The wavy imaginary central potential has regions in the surface where it is emissive (without breaking the unitarity

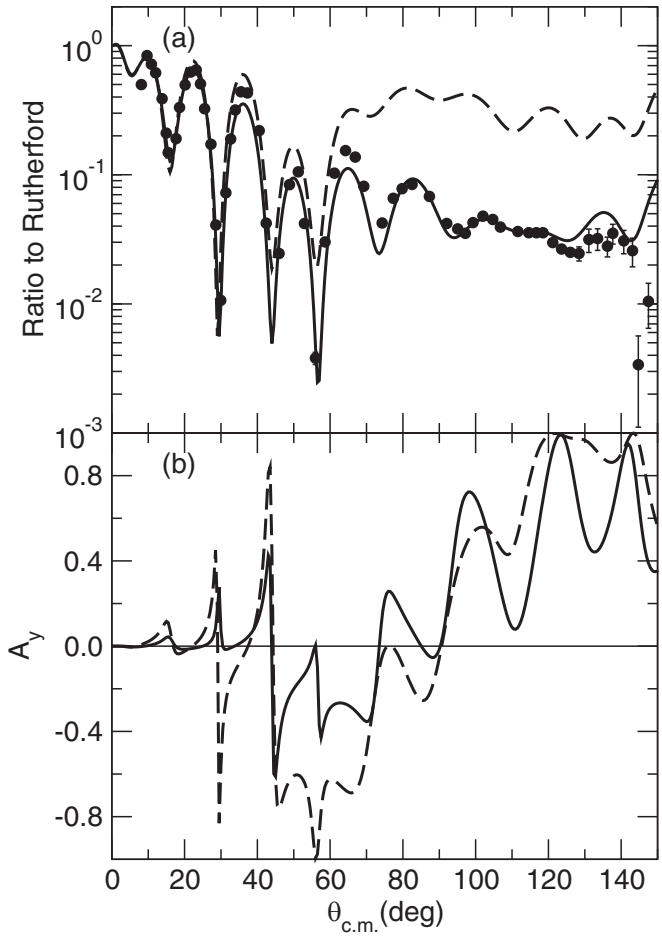

FIG. 2. For 33-MeV ^{3}H on ^{40}Ca, the solid lines are the differential cross-section (a) and analyzing power (b) angular distributions for the full coupled-channel calculation with fitted optical model parameters. The dashed lines are calculated with the same potential (the bare potential) but with no coupling. The data are from Ref. [31].

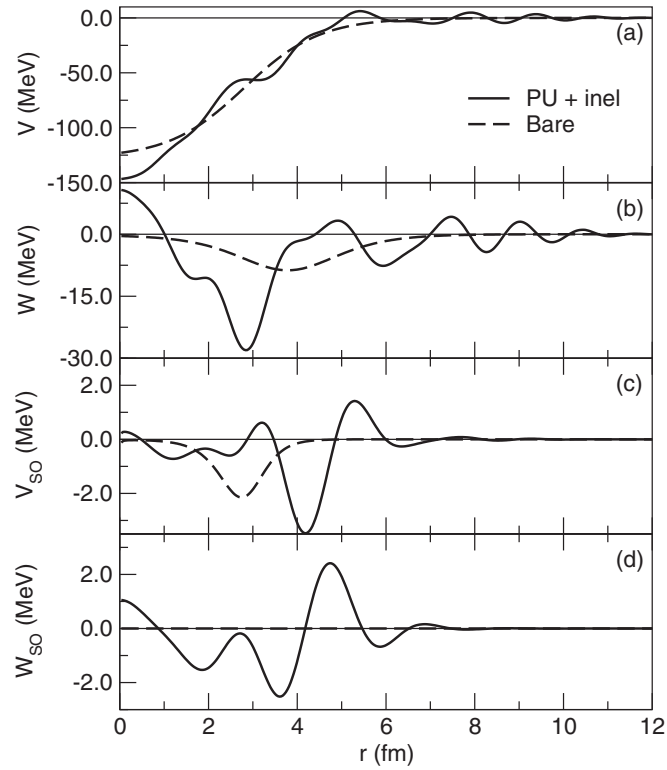

FIG. 3. For 33-MeV ^{3}H on ^{16}O, the bare potential (dashed lines) and the inverted potential including pickup and inelastic coupling contributions (solid lines). Labels (a), (b), (c), and (d) refer respectively to the real central, imaginary central, real spin-orbit, and imaginary spin-orbit components.

limit); the deep absorptive dip around 3 fm and the sharp change in the emissive direction at smaller r are familiar from the ^{3}He case.

(3) A strong, complex spin-orbit interaction has been generated. It is nothing like the usual Thomas form of the standard phenomenology, and such spin-orbit interactions will be a common property of all the DPPs that will follow.

It therefore appears that mass-3 spin-orbit interactions are dominated by channel coupling effects and nothing like either standard phenomenology or standard folding models.

TABLE I. For ^{3}H scattering from ^{16}O and ^{40}Ca at 33 MeV, volume integrals ΔJ (in MeV fm^3) of the four components of the DPP induced by (^{3}H, ^{4}He) pickup coupling ("PU") and/or coupling to inelastic states ("inel"). The coupled states for ^{16}O are specified in Sec. II B 1 and those for ^{40}Ca are specified in Sec. II B 2; the excitation energies of the states, in MeV, are all specified. The $\Delta R_{\rm rms}$ column gives the change in rms radius of the real central component (in fm). The final three columns present, respectively, the change in the total reaction cross section induced by the coupling, the integrated cross section to the specific coupled reaction channels, and the ratio R defined in the text. Note that negative $\Delta J_{\rm R}$ corresponds to repulsion. The quantities Δ(CS) and state CS are given in mb.

Line	Label	Coupling	$\Delta J_{\rm R}$	$\Delta J_{\rm IM}$	$\Delta J_{\rm RSO}$	$\Delta J_{\rm IMSO}$	$\Delta R_{\rm rms}$	Δ(CS)	State CS	R
1	PU on ^{16}O	$\frac{1}{2}^-$ and $\frac{3}{2}^-$	−18.34	24.01	0.5909	0.3735	−0.0312	26.6	20.28	1.108
2	Inel on ^{16}O	3^-	−39.48	21.29	0.3829	−0.6211	−0.0969	24.8	40.21	1.165
3	Inel and PU on ^{16}O	$\frac{1}{2}^-$, $\frac{3}{2}^-$, and 3^-	−55.93	17.14	2.1313	0.0460	−0.1892	33.4	49.41	1.948
4	Inel and PU summed		−57.82	45.30	0.9738	−0.2476	−0.1281	51.4	60.49	1.135
5	PU on ^{40}Ca	See text	−8.34	15.74	−0.197	0.075	−0.053	7.2	13.91	0.457
6	Inel on ^{40}Ca	See text	−17.99	17.03	−0.551	0.722	−0.028	8.7	24.18	0.511
7	Inel and PU on ^{40}Ca	See text	−18.95	20.72	−0.016	−0.270	0.122	9.5	35.57	0.459
8	Inel and PU summed		−26.33	32.77	−0.748	0.797	−0.081	15.9	38.09	0.485

IV. EVALUATING THE DPPs

The local equivalent DPPs are determined by subtracting the components of the bare potentials from the corresponding components of the potential determined by inverting S_{lj} for the elastic channel of the particular CC case being studied. Characteristic properties of the DPPs for various combinations of the possible coupling are presented in Table I in terms of the differences between corresponding properties of the inverted and bare potentials. The radial forms for the DPPs for ^{3}H on ^{16}O are presented in Sec. IV A, and those for ^{3}H on ^{40}Ca are presented in Sec. IV B.

In Table I we employ the standard normalization of Ref. [1] for J_R and J_I, the volume integrals of the real and imaginary potentials. We also adhere to the standard sign convention, in which a positive sign represents attraction or absorption. Thus, a negative value for ΔJ_R represents a repulsive contribution from the particular coupling in question. To get a measure of the magnitude of coupling effects, note that for ^{3}H on ^{16}O the volume integrals of the real and imaginary terms of the bare (uncoupled) potentials were, respectively, $J_R = 468.66$ MeV fm^3 and $J_{IM} = 110.06$ MeV fm^3. The corresponding values for scattering from ^{40}Ca were $J_R = 338.41$ MeV fm^3 and $J_{IM} = 77.07$ MeV fm^3. We remark that for ^{16}O both values are smaller in magnitude than for the ^{3}He case. However, the reverse is true for ^{40}Ca.

For each case, Table I also presents Δ(CS), the change in reaction cross section due to the coupling. The quantity R is the ratio of Δ(CS) to ΔJ_{IM}, the change due to coupling in the volume integral of the imaginary central potential:

$$R = \frac{\Delta(\mathrm{CS})}{\Delta J_{IM}}. \tag{1}$$

R varies over a much smaller range than Δ(CS) or ΔJ_{IM} separately. It will turn out that R exceeds unity for all ^{16}O cases but is around 0.5 for all ^{40}Ca cases.

Table I also presents the "state CS" which is the total (^{3}H, ^{4}He) and/or (^{3}H, ^{3}H$'$) cross section in mb to the pickup states and/or the collective states as specified in column 2. It gives a measure of the coupling and in some cases the magnitude varies more than, and sometimes contrariwise to, the corresponding ΔJ_{IM}. For ^{40}Ca in particular, the increase in reaction cross section, Δ(CS), is much less than the state CS in all cases, reminiscent of the suppression of fusion by inelastic processes.

Regarding the comparison of the DPPs for different couplings, it is important to note that all calculations for each target nucleus were carried out with a fixed bare potential: the potential that was determined by a search with all couplings included. The relative insensitivity of the DPP to the specific properties of the bare potential is presented in Ref. [8].

A. Radial forms of DPPs for ^{3}H on ^{16}O

Figure 4 presents the DPPs (i) for coupling to the pickup states (labeled "PU only," dashed lines), (ii) for coupling to the collective state (labeled "inel only," dotted lines), and (iii) for coupling to both the collective and transfer states (labeled "PU + inel," solid lines). There is no mutual coupling between the inelastic and pickup channels. The PU

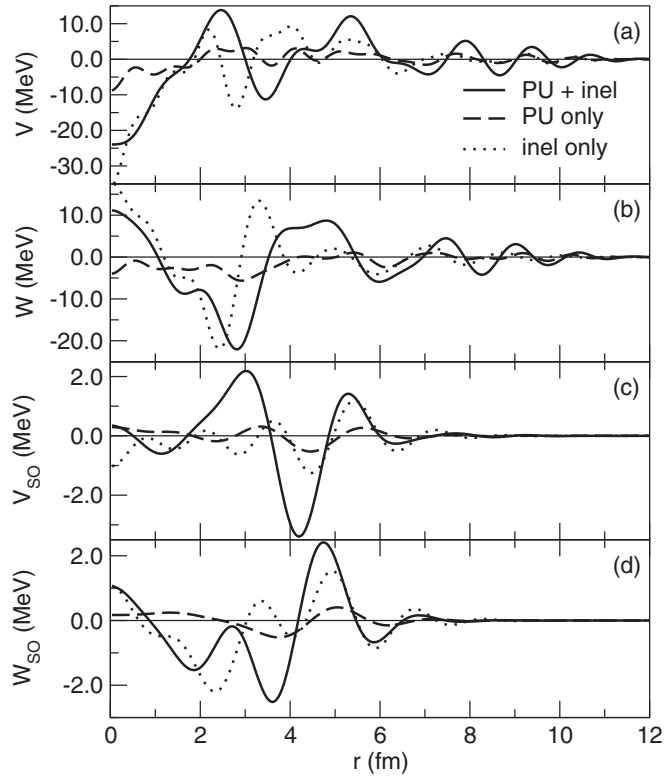

FIG. 4. For 33-MeV ^{3}H on ^{16}O, the DPPs for coupling to the 3$^-$ collective state "inel," dotted lines; to the two pickup states "PU," dashed lines; and both couplings, solid lines. Labels (a), (b), (c), and (d) refer respectively to the real central, imaginary central, real spin-orbit, and imaginary spin-orbit components.

case exhibits a shallow attractive region near the origin, and repulsion between about 2 and 6 fm. The overall effect is a net repulsion, $\Delta J_R = -18.34$ MeV fm^3 in line 1 of Table I, and a change in the rms radius of -0.0312 fm. The dotted line shows that inelastic coupling alone gives a much stronger attractive region at the nuclear center but overall repulsion further out and a corresponding decrease of the rms radius, -0.0969 fm. When pickup and inelastic coupling are included together, not only does the attraction at the nuclear center of the inelastic coupling persist, but the overall repulsion is increased as indicated by $\Delta J_R = -55.93$ MeV fm^3 in line 3 of Table I, and, as in all cases reported in Table I, the rms radius changes, in this case by -0.189 fm.

As might be expected the coupling increases the volume integral of the imaginary central potential, and for the full case (line 3) ΔJ_{IM} is just 17.14 MeV fm^3; this is conspicuously less than the sum, 45.30 MeV fm^3, of the increments ΔJ_{IM} due to pickup and inelastic coupling separately. This surprising effect was found in the ^{3}He case [4] and will be discussed in connection with Fig. 5 but we note here that both the inelastic and pickup coupling lead to somewhat undulatory (wavy) imaginary central components, the pickup DPP being less wavy than that due to inelastic coupling. This is a property that will also occur for the case of ^{40}Ca discussed below and was found for the ^{3}He case. The magnitudes of the cross sections to the coupled states (state CS) for PU or "inel" coupling

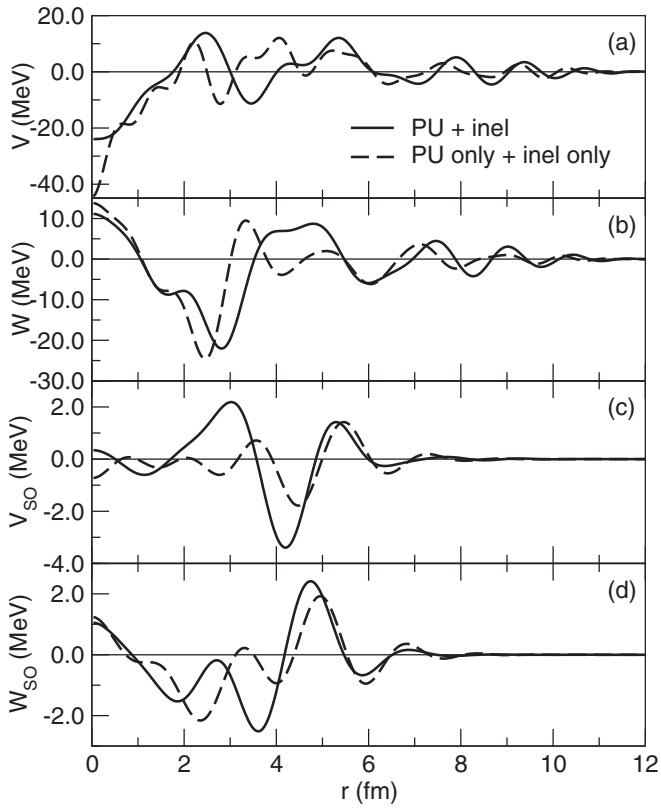

FIG. 5. For 33-MeV ^{3}H on ^{16}O, the solid lines present the DPP for coupling to both the pickup and collective states. The dashed lines present the numerical sums of the DPPs generated by each (collective or pickup) coupling separately. Labels (a), (b), (c), and (d) refer respectively to the real central, imaginary central, real spin-orbit, and imaginary spin-orbit components.

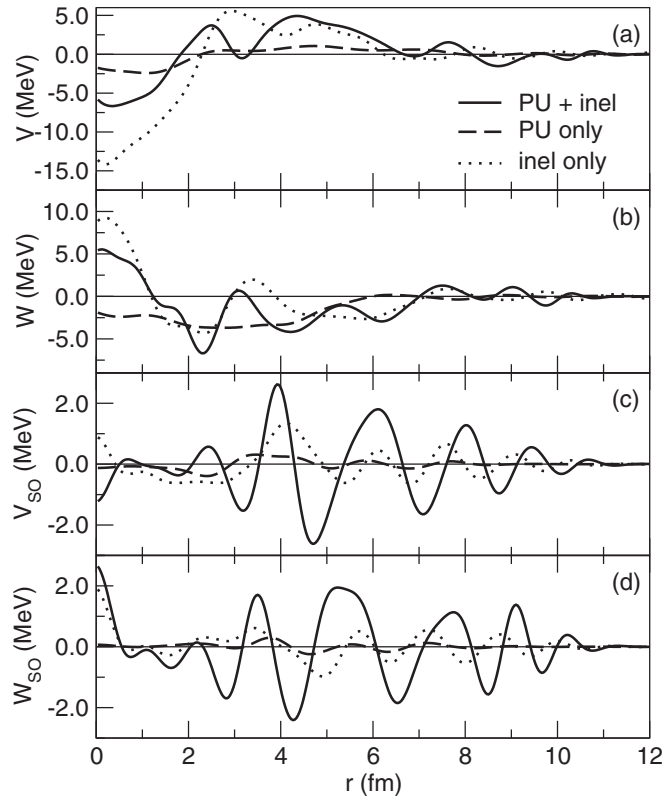

FIG. 6. For 33-MeV ^{3}H on ^{40}Ca, the DPPs for coupling to the 2^{+} and 3^{-} collective states "inel," dotted lines; to the pickup states "PU," dashed lines; and both couplings, solid lines. Labels (a), (b), (c), and (d) refer respectively to the real central, imaginary central, real spin-orbit, and imaginary spin-orbit components.

are not reflected in the changes in the imaginary potentials, as quantified by $\Delta J_{\rm IM}$. For ^{16}O $\Delta J_{\rm IM}$ is actually smaller for the inelastic coupling than for the pickup coupling although the cross section to the coupled inelastic state is a factor of 2 larger. The similar disconnect between state CS and $\Delta J_{\rm IM}$ for ^{40}Ca is less extreme.

We have seen that the volume integrals for the inelastic and pickup couplings do not add, and this applies point by point as shown in Fig. 5, which compares, for the four components, (i) the numerical sums of the local DPPs due to pickup and inelastic coupling and (ii) the local DPP when both couplings are operative together. While the general shapes of the central terms are visually similar, the differences are sufficient to lead to the differences in the volume integrals in Table I, although the r^2 weighting in the volume integral makes visual judgment difficult.

B. Radial forms of DPPs for ^{3}H on ^{40}Ca

Figure 6 presents the DPPs for coupling to the states specified in Sec. II B 2. The dashed lines present the DPPs due to coupling to the pickup states, the dotted lines are for inelastic coupling to the vibrational states, and the solid lines represent the components of the DPP when both inelastic and pickup couplings are included, with no mutual couplings between the collective and transfer channels. Certain general properties found in the ^{16}O case recur: concerning the real central term, both couplings generate attraction at the nuclear center but, as seen in Table I, the overall effect is repulsive. As was the case for ^{16}O, the attraction near $r = 0$ is greater for the inelastic coupling than for the pickup coupling, but the total effect in that region is smaller when both couplings are effective.

The inelastic coupling actually generates a DPP that is emissive from the center to 1 fm but, as can be seen from Table I, the effect on the volume integral is as strongly absorptive as the pickup term.

It is clear that the pickup and inelastic DPPs are of different character, and a full representation of the coupling effect requires the inclusion of both kinds of coupling. However, inelastic and transfer DPPs cannot be calculated separately and then added. This can be seen in Fig. 7, which compares the sum of the pickup and inelastic DPPs with the DPP when both couplings are included together. This is very significant since this nonadditivity is a direct consequence of the dynamical nonlocality of the underlying DPPs, of which the DPPs presented here are the local equivalents.

C. General properties of the DPPs

As will be seen in Figs. 4–7, all components of the DPPs have some degree of undularity, with some local regions

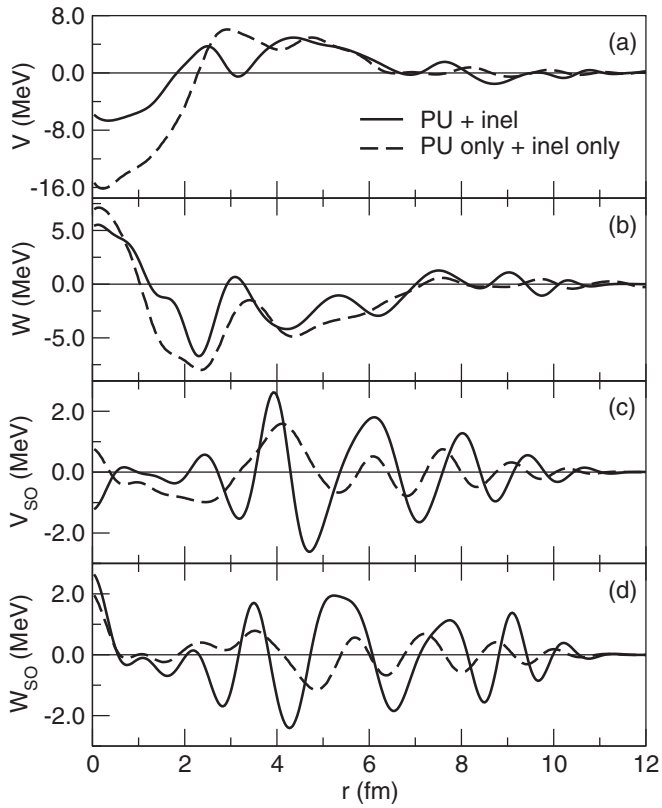

FIG. 7. For 33-MeV ^{3}H on ^{40}Ca, the solid lines present the DPP for coupling to both the pickup and collective states. The dashed lines present the numerical sums of the DPPs generated by each (collective or pickup) coupling separately. Labels (a), (b), (c), and (d) refer respectively to the real central, imaginary central, real spin-orbit, and imaginary spin-orbit components.

where the imaginary terms become emissive. This does not lead to any breaking of the unitarity limit.

Here we note systematic properties revealed in Table I and Figs. 4–7.

(1) In broad terms, coupling to both inelastic channels and pickup channels induces repulsion (negative $\Delta J_{\rm R}$) and absorption (positive $\Delta J_{\rm IM}$). However, the r dependence of the contribution due to inelastic coupling is systematically different from that due to pickup. Both are very far from representing a uniform renormalization of the bare potential.

(2) With one exception, the coupling (inelastic, pickup, or both together) causes a reduction in the rms radius of the real central term, i.e., $\Delta R_{\rm rms} < 0$. This is actually the opposite of the very systematic behavior found for protons on ^{40}Ca. This sensitivity is relevant to the extraction of nuclear sizes using nuclear scattering.

The first point, together with the general undularity of the DPPs, exposes what is lost by fitting folding model potentials to elastic-scattering data by uniform renormalization.

V. DYNAMICAL NONLOCALITY OF THE DPPs

We have stressed the fact that the DPPs generated by coupling are nonlocal, and that the DPPs presented here are their local equivalents and thus correspond to the contribution of the particular couplings to the local OMP. The products of most local density model folding calculations are local, and these generally have rather smooth radial forms. Such local phenomenological OMPs are, of course, key ingredients in distorted wave Born approximation (DWBA) analyses of transfer reactions. Although there is now a considerable literature on exchange-generated nonlocality in direct reactions, the dynamically generated nonlocality is quite distinct. In spite of its obvious significance for direct reactions, dynamical nonlocality has been little studied; for exceptions, see Refs. [16,17]; for further discussion, particularly of the nonadditivity property, see Ref. [21], where the additivity of the formal nonlocal DPPs is demonstrated. It is the dynamical nonlocality generated by the coupling to transfer and inelastic channels that leads to certain striking effects.

One such consequence of dynamical nonlocality, seen in the present paper, is the nonadditivity of local DPPs as deduced from the local potentials found by inversion. This can be seen in comparisons of line 3 and line 4 and of line 7 and line 8 of Table I. A direct indication of the dynamical nonlocality appears in a comparison of (^{3}H, ^{4}He) DWBA stripping calculations in which the ^{3}H propagates alternatively in a dynamically nonlocal potential or in the local equivalent potential. This provides a direct indication of the effects of dynamical nonlocality otherwise evidenced by the nonadditivity of local DPPs that are due to different couplings. This comparison sends a message about the importance of dynamical nonlocality in the analysis of direct reactions in which there is coupling to many states that are not mutually coupled but which can nevertheless have a mutual influence.

A difficulty in making such a comparison would, in general, be the requirement of calculating the ^{3}H wave function in the presence of a nonlocal potential. This would normally involve solving an integrodifferential equation, perhaps iteratively. This difficulty can be obviated by exploiting the fact that the wave function generated by the nonlocal DPP is, in fact, present in the CC calculations that generate the coupling. This can be exploited in the FRESCO [12] code by adding one-way pickup coupling between the ^{3}H wave function, effectively subject to a dynamically nonlocal potential, and a ^{4}He wave function in the exit partition.

This works out as follows in the examples we present here. We consider a DWBA (^{3}H, ^{4}He) pickup calculation on ^{16}O in which the ^{3}H wave function is calculated in two alternative ways: (i) in a coupled-channel calculation in which the elastic channel is coupled to the 3^- state of ^{16}O and (ii) as propagating in the local potential that includes the local equivalent of the implicit DPP due to the same coupling. We have done this for two states of ^{15}N: (1) the $\frac{1}{2}^-$ ground state (Q value 7.6865 MeV) and (2) the $\frac{3}{2}^-$ state at 6.3238 MeV (Q value 1.3627 MeV). Thus, in this case the dynamical nonlocality is that due only to the coupling to the collective state and not to PU processes. Note that the ^{3}H elastic-scattering observables are identical for both calculations. Results of this comparison are presented in Fig. 8. The upper panel presents the angular distributions for pickup leading to the $\frac{1}{2}^-$ ground state and the lower panel presents the comparison for pickup leading

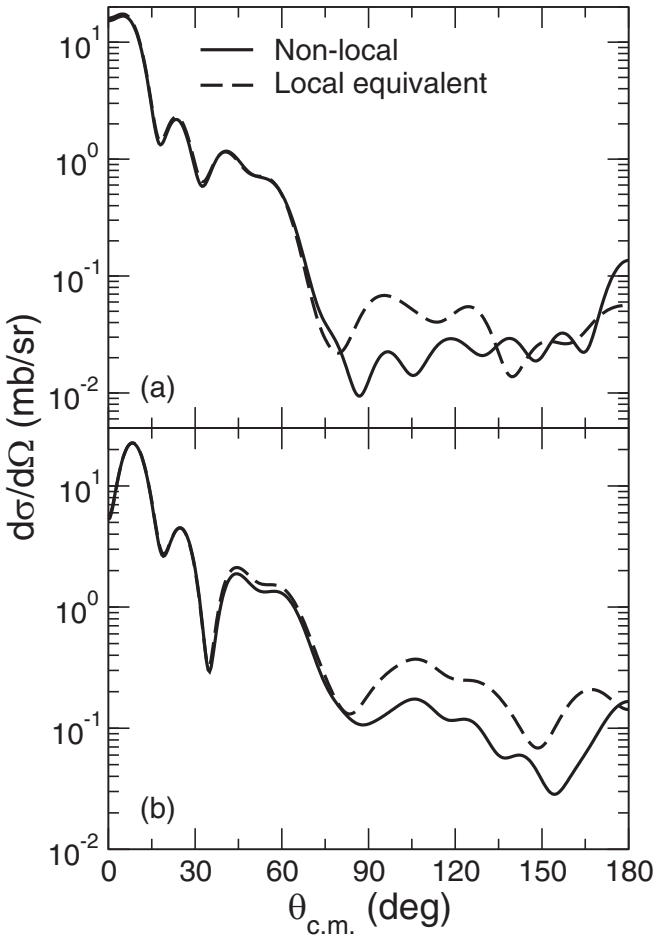

FIG. 8. For 33-MeV ^{3}H on ^{16}O, comparing DWBA calculations of (^{3}H, ^{4}He) pickup in which (i) the ^{3}H propagates in a dynamically nonlocal potential (solid lines) and (ii) the ^{3}H propagates in the local equivalent (dashed lines). The upper panel (a) is for neutron pickup leading to the $\frac{1}{2}^-$ ground state of ^{15}N and the lower panel (b) is for pickup to the $\frac{3}{2}^-$ state of ^{15}N, $E_x = 6.32$ MeV.

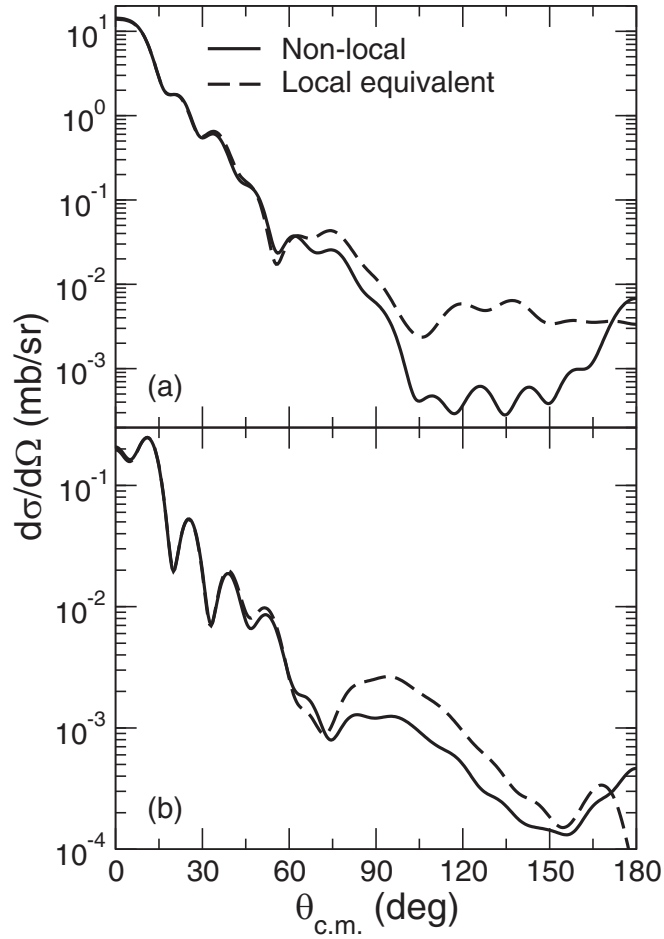

FIG. 9. For 33-MeV ^{3}H on ^{40}Ca, comparing DWBA calculations of (^{3}H, ^{4}He) pickup in which (i) the ^{3}H propagates in a dynamically nonlocal potential (solid lines) and (ii) the ^{3}H propagates in the local equivalent (dashed lines). The upper panel (a) is for neutron pickup leading to the $\frac{3}{2}^+$ ground state of ^{39}K and the lower panel (b) is for pickup to the $\frac{5}{2}^+$ state of ^{39}K, $E_x = 9.75$ MeV.

to the $\frac{3}{2}^-$ state at 6.3238 MeV. In each case the solid line corresponds to the triton propagating in a dynamically generated nonlocal potential and the dashed line is for ^{3}H propagation in the local equivalent potential. In the case of the ground state, the substantial difference in angular distribution starts at about 60° with the peak affected by about 5%. In the case of the $\frac{3}{2}^-$ excited state, the substantial difference starts around 40°.

We also consider a DWBA (^{3}H, ^{4}He) pickup calculation on ^{40}Ca in which the ^{3}H wave function is calculated in two alternative ways: (i) in a coupled-channel calculation in which the elastic channel is coupled to the 2^+ and 3^- states of ^{40}Ca as in the calculations reported above and (ii) as propagating in the local potential that includes the local equivalent of the implicit DPP due to the same coupling. We have done this for two states of ^{39}K: (1) the $\frac{3}{2}^+$ ground state (Q value 11.4857 MeV) and (2) the $\frac{5}{2}^+$ state at 9.75 MeV (Q value 1.74 MeV). Thus in this case the dynamical nonlocality is that due only to the coupling of the two collective states and not to PU processes. Note that the ^{3}H elastic-scattering observables are identical for both calculations. Results of these comparisons are presented in Fig. 9. The upper panel presents the angular distributions for pickup leading to the $\frac{3}{2}^+$ ground state and the lower panel presents the comparison for pickup leading to the $\frac{5}{2}^+$ state at 9.75 MeV. In each case the solid line corresponds to the triton propagating in a dynamically generated nonlocal potential and the dashed line is for ^{3}H propagation in the local equivalent potential. In the case of the ground state, the substantial difference in angular distribution starts at about 30°, the peak being affected by just 3%.

Regarding these two comparisons, if one demands a fit at all angles for assurance that the transfer calculation delivers accurate spectroscopic information, then even for the excited-state cases the difference is significant. However, for the ground-state cases, the result could be significant for the extraction of spectroscopic factors. These cases simultaneously demonstrate the reality of dynamically generated nonlocality and provide evidence of its significance in the analysis of direct reactions.

VI. COMPARISON WITH THE ^{3}He CASE

In the present paper we have closely followed, for the ^{16}O and ^{40}Ca targets, the most significant ^{3}He DPP calculations [4]. One motivation was the need to establish beyond reasonable doubt the importance of processes that appear to have no representation in current folding model calculations, or in any calculations based on a local density approximation. We appreciate that the effects we find are not straightforward to include in global models, dispersion consistent or otherwise. It seems worthwhile to establish that the general features of the DPPs and other effects that were found for the ^{3}He case recur for ^{3}H cases, with differences which are intelligible.

The Q values for ^{3}H pickup reactions are greater than those for ^{3}He pickup reactions, particularly so for the ^{40}Ca target. The pickup Q values for the ^{16}O target are 4.9137 MeV for ^{3}He and 7.6865 MeV for ^{3}H. For the ^{40}Ca target, the pickup Q values are 4.9426 MeV for ^{3}He and 11.4857 MeV for ^{3}H. The expectation, therefore, is that the DPPs due to pickup for ^{3}He and ^{3}H, while being qualitatively similar, should have systematically different overall magnitudes. It turns out that magnitudes of the DPPs decrease with increasing Q value, the ^{3}He pickup DPPs being systematically larger than for ^{3}H, although the patterns are similar: comparing Table I with Table I of Ref. [4] we find a very similar pattern of contributions. Some key points are as follows.

(1) (relating to the ^{16}O case) Pickup coupling results in ΔJ_R, ΔJ_{IM}, and ΔR_{rms} all having the same sign as for ^{3}He scattering but, for each quantity, a somewhat smaller magnitude. This might be related to the larger PU Q value for ^{3}H (about 7.7 MeV compared with 4.9 MeV for ^{3}He). Both Δ(CS) and state CS are smaller in magnitude than for ^{3}He but Δ(CS) differs from state CS, following the same pattern as for ^{3}He.

(2) (relating to the ^{16}O case) Inelastic (inel) coupling results in ΔJ_R, ΔJ_{IM}, and ΔR_{rms} all having the same sign as for ^{3}He but in this case while ΔJ_R and ΔR_{rms} are smaller in magnitude than for ^{3}He (but still substantially reducing the attraction) ΔJ_{IM} is larger in magnitude. Both Δ(CS) and state CS are smaller in magnitude than for ^{3}He but for the inel case Δ(CS) is less than state CS, as it was for ^{3}He.

(3) (relating to the ^{40}Ca case) Pickup coupling results in ΔJ_R, ΔJ_{IM}, and ΔR_{rms} all having the same sign as for ^{3}He scattering but, for each quantity, a somewhat smaller magnitude. This might be related to the larger PU Q value for ^{3}H (about 11.5 MeV compared with 4.9 MeV for ^{3}He). Both Δ(CS) and state CS are smaller in magnitude than for ^{3}He and also much smaller than for ^{3}H on ^{16}O. As was the case for ^{3}He, Δ(CS) is less than state CS.

(4) (relating to the ^{40}Ca case) Inelastic (inel) coupling results in ΔJ_R, ΔJ_{IM}, and ΔR_{rms} all having the same sign as for ^{3}He but in this case while ΔJ_R and ΔR_{rms} are smaller in magnitude than for ^{3}He (but still substantially reducing the attraction) ΔJ_{IM} is larger in magnitude. Both Δ(CS) and state CS are smaller in magnitude than for ^{3}He but for the inel case Δ(CS) is less than state CS, as it was for ^{3}He.

(5) A remarkable feature that is common to both the ^{16}O and ^{40}Ca cases is the small magnitude of ΔJ_{IM} (and to a lesser extent of ΔJ_R), for the cases when inel and PU couplings are both included compared to the summed contributions of PU coupling and inel coupling separately. Exactly the same effect was found for ^{3}He in Ref. [4]. This is related to the nonadditivity of the local equivalents of the formal nonlocal dynamical DPPs, as discussed below.

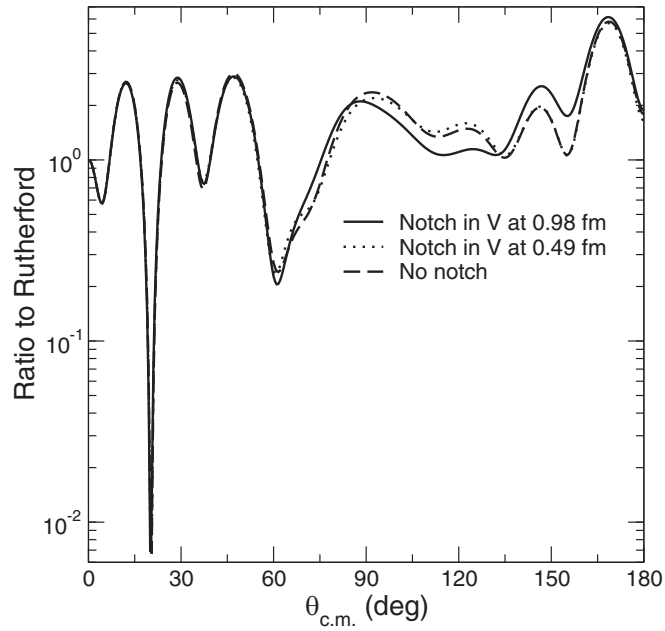

FIG. 10. For 33-MeV ^{3}He on ^{16}O, the angular distribution with the full potential without a notch (dashed line), the angular distribution for the same potential but with a notch at 0.49 fm (dotted line), and with a notch at 0.98 fm (solid line).

Note that, unlike all the other properties, calculations of Δ(CS) and state CS are not affected by the S-matrix inversion. The naive expectation would be that the reaction cross section will increase, when a coupling is turned on, by the magnitude of the cross section to the coupled state. In fact, the outcome is different in a way that is the same for ^{3}He and ^{3}H; i.e., for PU on ^{16}O, Δ(CS) is greater than state CS, but for all other cases for ^{3}He as well as ^{3}H state CS is greater than Δ(CS).

VII. SENSITIVE RADIAL RANGE

While the inversion process yields DPPs with significant magnitudes at radii down to $r = 0$ it is legitimate to pose the question whether the potential near the nuclear center matters for ^{3}H on ^{16}O or ^{40}Ca at 33 MeV. It is reasonable to ask whether features in the region of $r = 0$ of the potential, such as for the ^{16}O case in Fig. 3 (see also Fig. 5, solid lines), could have a significant effect on scattering. To answer this, we present the results of "notch" tests for the ^{16}O case in Fig. 10 and for the ^{40}Ca case in Fig. 11. For the ^{16}O case the figure compares the angular distribution for the full potential of Fig. 3 and (implicitly) Fig. 5 with the angular distributions when the same potential has deep notches in the real part at 0.49 and 0.98 fm. The notches were of Gaussian form of width 0.025 fm and depth equal to the full potential at the central point of the notch. Since the full potentials were tabulated in steps of 0.035 fm this amounted to almost V-shaped notches.

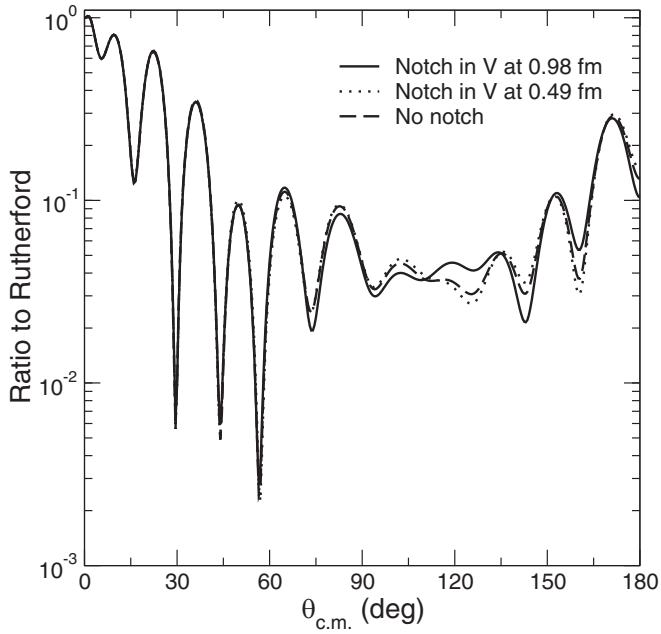

FIG. 11. For 33-MeV ^{3}H on ^{40}Ca, the angular distribution with the full potential without a notch (dashed line), the angular distribution for the same potential but with a notch at 0.49 fm (dotted line), and with a notch at 0.98 fm (solid line).

A similar comparison is made in Fig. 11 for ^{40}Ca and the full potential corresponding to the "PU + inel" case DPP of Fig. 7 (solid lines). From Fig. 11 we see that for ^{40}Ca there is substantial sensitivity around 1 fm and appreciable sensitivity even at 0.5 fm. This suggests that the radial shapes of the DPPs presented above are a realistic representation of the effect of channel coupling almost to the nuclear center. From Fig. 10 there is even more sensitivity when the separation of the ^{3}H and ^{16}O is very small.

VIII. OMITTED PROCESSES AND FUTURE EXTENSIONS

This paper has shown once more that reaction and inelastic channel couplings make substantial contributions to the elastic-scattering OMP. The local equivalent contributions generally have an undulatory radial dependence in all components and hence cannot be represented as a uniform renormalization of, or smooth addition to, a folding model potential. The coupling contributions seem to have no representation in current folding models, suggesting that a comprehensive study of such contributions is required. The present paper is a small step in this direction. To name one omission, it is likely that, for example, one nucleon stripping and perhaps two nucleon stripping would make contributions of a comparable magnitude.

Establishing a more general account of the contribution of channel coupling is made more difficult by a particular consequence of the nonlocality of the formal (nonlocal and l-dependent) DPPs that are generated by coupling. The local DPPs that are due to any individual couplings cannot simply be added to yield the local and l-independent DPP due to all those couplings when included simultaneously. This is because, referring to DPPs due to particular couplings, the sum of local equivalents is not the local equivalent of sums. As a result, a comprehensive calculation of all processes that might make a substantial contribution will require a single CC calculation that includes all significant coupled states. This applies even with no explicit coupling between contributing channels.

For reasons indicated in Sec. VI, the present paper has been confined to $T = 0$ targets. One obvious extension would be a comparison of pickup contributions to the OMPs for ^{3}He and ^{3}H scattering from ^{48}Ca; it is likely that the ^{3}He pickup DPPs would be larger than ^{3}H pickup DPPs in this case. More generally, we need to have some measure of the contribution of pickup coupling for heavier nuclei. For ^{3}He scattering from ^{208}Pb the DPPs, while smaller in magnitude than those for ^{40}Ca, were still appreciable [4]. A particular challenge is to account for the difference between global potentials and potentials local to closed shells, as found for ^{3}He in Ref. [13]

IX. SUMMARY AND CONCLUSIONS

There are detailed similarities between the channel coupling contributions for ^{3}H scattering on ^{16}O and ^{40}Ca and the corresponding contributions for ^{3}He scattering as presented in Ref. [4]. The nature of the contributions is further evidence that folding models based on local density models lack a representation of substantial basic properties of the local OMP.

The irregular shapes (waviness or undularity) of the local and l-independent representations of the DPPs make it clear that folding model potentials cannot adequately be tested by attempting to fit data with a uniform renormalization. A model-independent fit to elastic-scattering data with an additive term could provide independent evidence for the radial shapes that should be the target of reaction theory. There is already some evidence for undularity appearing in model independent fits to elastic-scattering data. Unfortunately, such was the prejudice against unsmooth potentials, that such fits were sometimes dismissed. The local DPPs arising from channel coupling lead to a modification of the rms radius of the real part. This is consistent with the general observation from studies of the present kind that coupling effects can undermine the use of elastic scattering for measurement of nuclear radii.

The coupling contributions to the real and imaginary spin-orbit interactions are undulatory and large, exceeding the bare spin-orbit potential in magnitude. This was also the case for ^{3}He scattering [4], and deserves further study. One line of inquiry would be to study the limits of the inversion while holding the spin-orbit potential fixed at the bare potential form by excluding spin-orbit terms from the inversion process. Concerning the comparison with the bare spin-orbit potential, we note that this potential is small in magnitude, about a third of the proton spin-orbit potential. From Table I it seems that for both ^{16}O and ^{40}Ca the inelastic coupling makes a contribution comparable to that of pickup, and the inelastic and pickup contributions do not add when both are active.

The nonadditivity of the *local* DPPs is a conspicuous feature of our results and is evidence of the strong dynamical nonlocality of the polarization potentials generated by the

coupling. The fact that the local equivalent of a sum of nonlocal potentials is not the sum of the local equivalents of each potential has been discussed in earlier work including Ref. [4] but is an unmistakable property of the volume integrals in Table I. It can also be seen in certain properties in Table I that are wholly independent of S-matrix inversion. The quantity state CS, the integrated cross section to the included inelastic or transfer states, does not add. For the ^{16}O target the sum of the state CS values for inelastic scattering and pickup is 60.49 mb, but the integrated cross section to the inelastic and pickup states when both are included is 49.41 mb. A similar, though not so dramatic, effect is seen with the ^{40}Ca target. Moreover the values of the change in total reaction cross section, Δ(CS), also do not add. This consequence of the substantial mutual influence between channels that are not coupled is an important finding of the present paper, and can be attributed to the dynamical nonlocality generated by the coupling. A further consequence of the dynamical nonlocality is manifested in the effect on pickup reactions as shown in Figs. 8 and 9.

Nuclear theory is undergoing rapid development with the introduction of effective field theories and the exploitation of *ab initio* methods that are enabled by increased computer power. What we have shown in this paper implies that the developing theory of the interactions between nuclei must include some representation of the transfer of nucleons, or nuclear clusters, between the nuclei. The effects of excitations of the nuclei as they mutually interact must also be included. This is exemplified by the contribution to the elastic scattering of ^{3}H of the coupling to states involving the transfer of a proton and the coupling to excited states of the target nucleus. The local density model, which is the basis of almost all folding model calculations of OMPs, cannot be fully valid. This is particularly manifest in the shapes of the DPPs generated by the coupling both to transfer channels and to excitations of the interacting nuclei. These wavy shapes bear little connection to the radial density of the nucleus. There has never been a challenge to the reaction theory that leads via established S-matrix inversion to undularity. Unfortunately, model independent fits that do lead to undularity tend to be ignored, or the parameter search is halted at the point where undularity is emerging. Undularity inevitably appears in the potentials that are l-independent S-matrix equivalents of those l-dependent potentials that give precise fits to elastic-scattering data. For a review of l dependence of nuclear OMPs, see Ref. [32]. Direct evaluation of the formal contribution of excitations to nuclear OMPs leads (see, e.g., Ref. [3]) to highly nonlocal and l-dependent potentials that cannot easily be related to phenomenological potentials and such calculations are rarely pursued.

[1] G. R. Satchler, *Direct Nuclear Reactions* (Clarendon, Oxford, 1983).
[2] H. Feshbach, Ann. Phys. (NY) **5**, 357 (1958); **19**, 287 (1962).
[3] G. H. Rawitscher, Nucl. Phys. A **475**, 519 (1987).
[4] R. S. Mackintosh and N. Keeley, Phys. Rev. C **100**, 064613 (2019).
[5] R. S. Mackintosh and N. Keeley, Phys. Rev. C **85**, 064603 (2012).
[6] N. Keeley and R. S. Mackintosh, Phys. Rev. C **97**, 014605 (2018).
[7] R. S. Mackintosh and N. Keeley, Phys. Rev. C **97**, 069901(E) (2018).
[8] R. S. Mackintosh and N. Keeley, Phys. Rev. C **98**, 024624 (2018).
[9] N. Keeley and R. S. Mackintosh, Phys. Rev. C **99**, 034614 (2019).
[10] N. Keeley and R. S. Mackintosh, Phys. Rev. C **77**, 054603 (2008).
[11] A. M. Kobos and R. S. Mackintosh, Acta Phys. Pol. B **8**, 887 (1977).
[12] I. J. Thompson, Comput. Phys. Rep. **7**, 167 (1988).
[13] D. Y. Pang, P. Roussel-Chomaz, H. Savajols, R. L. Varner, and R. Wolski, Phys. Rev. C **79**, 024615 (2009).
[14] J. S. Hanspal, R. J. Griffiths, and N. M. Clarke, Phys. Rev. C **31**, 1138 (1985).
[15] R. S. Mackintosh, Scholarpedia **7**, 12032 (2012).
[16] R. S. Mackintosh and N. Keeley, Phys. Rev. C **81**, 034612 (2010).
[17] N. Keeley and R. S. Mackintosh, Phys. Rev. C **90**, 044602 (2014).
[18] F. G. Perey and B. Buck, Nucl. Phys. **32**, 353 (1962).
[19] F. G. Perey, in *Direct Interactions and Nuclear Reaction Mechanisms*, edited by E. Clemental and C. Villi (Gordon and Breach, New York, 1963), p. 125.
[20] R. S. Mackintosh and S. G. Cooper, J. Phys. G **23**, 565 (1997).
[21] R. S. Mackintosh and N. Keeley, arXiv:1610.07378.
[22] I. Brida, S. C. Pieper, and R. B. Wiringa, Phys. Rev. C **84**, 024319 (2011).
[23] F. Flavigny, A. Gillibert, L. Nalpas, A. Obertelli, N. Keeley, C. Barbieri, D. Beaumel, S. Boissinot, G. Burgunder, A. Cipollone, A. Corsi, J. Gibelin, S. Giron, J. Guillot, F. Hammache, V. Lapoux, A. Matta, E. C. Pollacco, R. Raabe, M. Rejmund, N. de Séreville, A. Shrivastava, A. Signoracci, and Y. Utsuno, Phys. Rev. Lett. **110**, 122503 (2013).
[24] C. Pinder, C. O. Blyth, N. M. Clarke, D. Barker, J. B. A. England, B. R. Fulton, O. Karban, M. C. Mannion, J. M. Nelson, C. A. Ogilvie, L. Zybert, R. Zybert, K. I. Pierce, P. J. Simmonds, and D. L. Watson, Nucl. Phys. A **533**, 25 (1991).
[25] V. Avrigeanu, M. Avrigeanu, and C. Mănăilescu, Phys. Rev. C **90**, 044612 (2014).
[26] T. Kibédi and R. H. Spear, At. Data Nucl. Data Tables **80**, 35 (2002).
[27] E. Strano, D. Torresi, M. Mazzocco, N. Keeley, A. Boiano, C. Boiano, P. Di Meo, A. Guglielmetti, M. La Commara, P. Molini, C. Manea, C. Parascandolo, D. Pierroutsakou, C. Signorini, F. Soramel, D. Filipescu, A. Gheorghe, T. Glodariu, J. Grebosz, S. Jeong, Y. H. Kim, J. A. Lay, H. Miyatake, M. Nicoletto, A. Pakou, K. Rusek, O. Sgouros, V. Soukeras, L. Stroe, N. Toniolo, A. Vitturi, Y. Watanabe, and K. Zerva, Phys. Rev. C **94**, 024622 (2016).
[28] P. Doll, G. J. Wagner, K. T. Knopfle, and G. Mairle, Nucl. Phys. A **263**, 210 (1976).

[29] S. Raman, C. W. Nestor, Jr., and P. Tikkanen, At. Data Nucl. Data Tables **78**, 1 (2001).
[30] R. S. Mackintosh and N. Keeley, Phys. Rev. C **90**, 044601 (2014).
[31] J. B. A. England, L. Zybert, G. T. A. Squier, O. Karban, R. Zybert, J. M. Nelson, D. Barker, B. R. Fulton, M. C. Mannion, C. A. Ogilvie, L. Potovin, C. Pinder, C. O. Blyth, G. C. Morrison, G. J. Pyle, S. Roman, N. M. Clarke, K. T. Pearce, P. J. Simmonds, R. J. Griffiths, D. L. Watson, M. D. Cohler, R. Wadsworth, J. O'Donnell, and M. Smithson, Nucl. Phys. A **475**, 422 (1987).
[32] R. S. Mackintosh, Eur. Phys. J. A **55**, 147 (2019).